Meteoritics & Planetary Science 40, Nr 3, 461–475 (2005)
Abstract available online at http://meteoritics.org

A unique type B inclusion from Allende with evidence for multiple stages of melting

S. B. SIMON,[1*] L. GROSSMAN,[1, 2] and A. M. DAVIS[1, 2]

[1]Department of the Geophysical Sciences, 5734 South Ellis Avenue, The University of Chicago, Chicago, Illinois 60637, USA
[2]The Enrico Fermi Institute, 5640 South Ellis Avenue, The University of Chicago, Chicago, Illinois 60637, USA
[*]Corresponding author. E-mail: sbs8@midway.uchicago.edu

(Received 29 July 2004; revision accepted 17 December 2004)

Abstract–A large (7 mm in diameter) Allende type B inclusion has a typical bulk composition and a unique structure: a fassaite-rich mantle enclosing a melilite-rich core. The core and mantle have sharply contrasting textures. In the mantle, coarse (~1 mm across), subhedral fassaite crystals enclose radially oriented melilite laths about 500 μm long that occur at the inclusion rim. The core consists of blocky melilite grains 20–50 μm across and poikilitically enclosed in anhedral fassaite grains that are optically continuous over ~1 mm. Another unique feature of this inclusion is that melilite laths also extend from the core into the mantle. Fassaite in both the core and mantle is very rich in fine-grained (1–10 μm) spinel. The rim laths are normally zoned ($Åk_{30–70}$) inward from the rim of the inclusion with reverse zoning over the last ~200 μm to crystallize. A very wide range of melilite compositions is found in the core of the inclusion, where gehlenitic grains ($Åk_{5–12}$) occur. These grains are enclosed in strongly zoned ($Åk_{15–70}$) overgrowths. The gehlenitic cores and innermost parts of the overgrowths are Na_2O-free, but the outer parts of the overgrowths are not. In the laths at the rim, Na_2O decreases inward from the rim, then increases. Fassaite in the core has the same range of Ti contents as that in the mantle: 2–9 wt% $TiO_2 + Ti_2O_3$. Two melting events are required to account for the features of this inclusion. In the first event, the precursor assemblage is heated to ~1400 °C and melts except for gehlenitic ($Åk_{5–12}$) melilite and some spinel. These grains become concentrated in the core. During cooling, Na_2O-free melilite nucleates at the rim of the inclusion and on the relict grains in the core. After open system secondary alteration, the inclusion is heated again, but only to ~1260 °C. Melilite more gehlenitic than $Åk_{40}$ does not melt. During cooling, Na_2O-bearing melilite crystallizes as small, blocky grains and laths in the core and as overgrowths on relict grains in the core and at the rim. Eventually melilite co-crystallizes with fassaite, leading to the reverse zoning observed in the laths. The coexistence in this inclusion of Na-free and Na-bearing melilite, plus a positive correlation between Na_2O and åkermanite contents in melilite in an inclusion with a bulk Mg isotopic composition that is mass-fractionated in favor of the heavy isotopes, are both consistent with at least two melting events. Several other recently described coarse-grained inclusions also have features consistent with a sequence of early, high-temperature melting, secondary alteration, and remelting at a lower temperature, suggesting that remelting of refractory inclusions was a common occurrence in the solar nebula.

INTRODUCTION

Refractory inclusions in carbonaceous chondrites consist of some of the first phases predicted to condense from a cooling gas of solar composition. The inclusions that compose one of the major types of coarse-grained, Ca- and Al-rich refractory inclusions (CAIs), the type Bs, consist of melilite, spinel, the Ti- and Al-rich variety of clinopyroxene known as fassaite (Dowty and Clark 1973), and anorthite. The type Bs are divided into two textural subtypes, B1s and B2s, depending upon the presence (B1) or absence (B2) of a continuous, nearly monomineralic mantle of melilite laths, predominantly radially oriented and grown inward from the rims of inclusions, enclosing a pyroxene-rich core. Type B2 inclusions have a relatively homogeneous distribution of phases. Some type B inclusions have thin, discontinuous mantles and could be classified as either B1 or B2, but most fall into one group or the other. The Allende inclusion

described herein, however, named Golfball, has the mineralogy and bulk composition of a type B inclusion, but has a structure that is unique among all samples that have been described: it has a very melilite-rich core and a pyroxene-rich mantle.

In typical type B1s, the earliest formed, most gehlenitic (Al_2O_3-rich) melilite occurs at inclusion rims, but in Golfball, the most gehlenitic melilite occurs in the core. This feature and the texture of the inclusion record a complex thermal history. Studies of such inclusions are important because they provide insight into sequences of solar nebular processes to which refractory condensates were exposed. Through continued petrographic and theoretical studies of refractory inclusions, a picture is emerging that some of them formed by partial evaporation of melted condensate assemblages (Grossman et al. 2000, 2002; Richter et al. 2002). Furthermore, there is strong evidence, to which this report adds, that at least some type B CAIs have melted more than once (MacPherson and Davis 1993; Beckett et al. 2000). As more is learned about the thermal histories of inclusions, the range of conditions to which refractory inclusions were exposed in the early solar nebula becomes better understood. We report here the results of a detailed study of Golfball and present a model that accounts for its features. Preliminary results of this study were reported by Simon et al. (2002) and Golfball is among the suite of inclusions, the bulk compositions of which were reported by Simon and Grossman (2004).

ANALYTICAL METHODS

The large (7 mm in diameter), spherical inclusion was recovered intact from an Allende hand sample. Approximately half was powdered and aliquots taken for bulk chemical and isotopic analysis; three thin sections were made from the other half. Two of the sections (GBL1, GBL2) sampled large-area, nearly equatorial, rim-to-rim planes. The remaining section (GBS) contains a smaller, crescent-shaped piece. Sections were studied with a JEOL JSM-5800LV scanning electron microscope (SEM) equipped with an Oxford/Link ISIS-300 energy-dispersive X-ray analysis system. The SEM was used to obtain backscattered electron images, qualitative elemental X-ray maps, and quantitative maps of åkermanite contents of melilite and TiO_2 contents of fassaite. Quantitative wavelength-dispersive analyses were obtained with a Cameca SX-50 electron microprobe operated at 15 kV with a beam current of 25 nA. Data were reduced via the modified ZAF correction procedure PAP (Pouchou and Pichoir 1984).

The major element (CaO, MgO, Al_2O_3, SiO_2, TiO_2, or CMAST) bulk composition was determined from the two large-area thin sections by modal recombination and is reported in Simon and Grossman (2004). Compositions of the core and mantle were calculated separately and combined according to their weight proportions to obtain a "raw" bulk composition for the inclusion (22.27 wt% CaO, 14.04 MgO, 33.59 Al_2O_3, 27.65 SiO_2, and 2.45 TiO_2). This result was corrected to the solar CaO/Al_2O_3 ratio by mathematical subtraction of spinel and addition of melilite and fassaite, as described by Simon and Grossman (2004), yielding a corrected bulk composition of 24.12 wt% CaO, 12.96 MgO, 30.46 Al_2O_3, 29.76 SiO_2, and 2.69 TiO_2.

RESULTS

Petrography

The unusual structure of this inclusion is apparent from the near-equatorial thin sections. Unlike any previously described inclusion, the core of Golfball is dominated by melilite and its mantle by fassaite (Fig. 1a). While this structure is unique, what makes this inclusion even more intriguing is the presence of melilite laths protruding from the core into the mantle (Figs. 1a and 1b). They are attached to the core at one end, enclosed by mantle fassaite at the other, and contain abundant inclusions of fine-grained spinel.

In addition to these laths, melilite occurs in the core as blocky grains 20–50 μm across separated by pockets of fassaite, spinel, and relatively rare anorthite, creating a spongy texture (Fig. 1c). Some melilite grains are poikilitically enclosed by fassaite that is optically continuous over ~1 mm. Except for that in the melilite laths, spinel in the core is almost entirely enclosed by fassaite; relatively little is enclosed by blocky melilite. A similar texture with pockets of spinel-rich fassaite amidst spinel-poor melilite has also been observed in a type B inclusion from Ningqiang (Lin and Kimura 2000).

Yet another unusual feature of Golfball is its vesicular mantle. Cavities in the mantle, such as those visible in Fig. 1a, are not artifacts and were observed in the sample prior to sectioning. They do not appear to be lined with any vapor-deposited grains. Parts of the rim and mantle are missing from the section because the presence of the cavities led to crumbling during sampling. The fassaite-rich, spinel-rich zone of the mantle is ~1 mm wide and consists of coarse (~1 mm), subhedral to nearly euhedral fassaite enclosing rounded to euhedral spinel grains that are mostly ≤20 μm across. Dense knots of coarse spinel, known as framboids (El Goresy et al. 1979), opaque assemblages termed Fremdlinge (El Goresy et al. 1979), FeNi metal, and pentlandite occur enclosed in the fassaite. Trace amounts of primary, anhedral anorthite occur in the mantle, typically adjacent to coarse fassaite grains.

In GBS, one of the sections that is not shown, the mantle contains one large (1.25 mm in diameter), spherical spinel palisade body (Wark and Lovering 1982) that is dominated by melilite laths 100–200 μm long. Coarse (~100 μm), anhedral fassaite occurs interstitial to the melilite. Unlike the spinel-

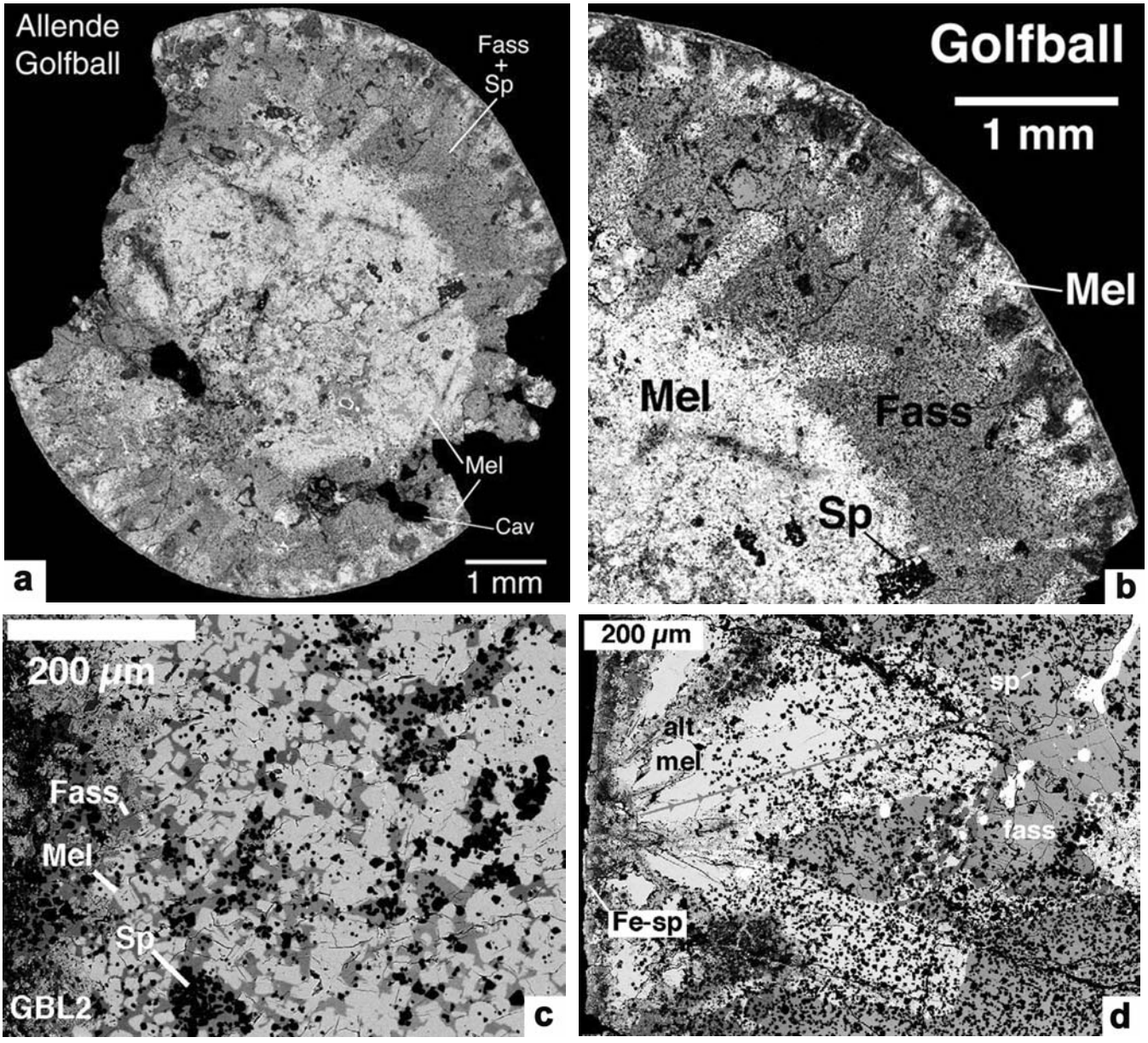

Fig. 1. Backscattered electron images of Golfball, section GBL2: a) Low-magnification view of a cross-section of the inclusion. Note the fassaite-rich mantle enclosing the melilite-rich core, and melilite laths protruding from the core into the mantle and inward from the rim of the inclusion. b) Higher-magnification view of a portion of the section shown in (a), showing melilite at the rim and in the core, with the fassaite-rich mantle between. c) Higher-magnification view of the core, showing the spongy texture of spinel-rich fassaite pockets among blocky melilite grains. d) A spray of melilite laths adjacent to the rim of the inclusion. The location and direction of an electron probe traverse is indicated by the arrowed line. Alt = alteration products; Cav = cavity; Fass = fassaite; Fe-sp = FeO-bearing spinel; Mel = melilite; Sp = spinel.

rich fassaite elsewhere in the inclusion, the fassaite in the palisade body is spinel-free, and in general, the interior of the palisade body is quite spinel-poor compared to the rest of the inclusion. The palisade body has many small, round, opaque assemblages consisting of FeNi metal ± sulfide ± magnetite. Like the rest of the inclusion, there is very little anorthite, and secondary alteration products of melilite are very common along veins and grain boundaries.

In addition to the ones in the core, radially-oriented melilite laths also occur at the smooth, rounded, outer edge of the inclusion in a thin, nearly continuous band. A spray of such crystals is shown in Fig. 1d. Like many of the other melilites at the rim, these crystals are ~500 μm long, have faceted terminations, and are largely enclosed in the massive fassaite that dominates the mantle of the inclusion. This inclusion therefore contains melilite laths that protrude inward from the edge of the inclusion toward the core and laths that protrude outward from the core toward the edge of the inclusion.

The outermost ~100 μm of the inclusion are very rich in

Table 1. Electron microprobe analyses of melilite in Golfball.

	1	2	3	4	5
Na_2O	BDL	0.13	0.18	0.08	0.19
MgO	1.05	6.39	8.78	4.75	8.77
Al_2O_3	34.81	20.24	14.77	24.28	13.98
SiO_2	22.97	31.07	34.78	28.69	34.77
CaO	41.58	41.34	41.00	41.41	41.34
TiO_2	BDL	BDL	BDL	0.04	BDL
FeO	n.a.	n.a.	0.08	0.05	0.28
Total	100.43	99.17	99.60	99.29	99.35
			Cations per seven oxygen anions		
Na	0	0.012	0.016	0.007	0.017
Mg	0.071	0.439	0.599	0.326	0.602
Al	1.870	1.099	0.797	1.318	0.758
Si	1.047	1.432	1.592	1.322	1.601
Ca	2.030	2.041	2.011	2.045	2.039
Ti	0	0	0	0.001	0
Fe	–	–	0.003	0.002	0.011
Total cations	5.018	5.024	5.018	5.021	5.028
Åk (mol%)	6.1	44.1	59.7	33.0	60.8

1 = Gehlenitic melilite in core; 2 = overgrowth on gehlenitic melilite in core; 3 = lath in core; 4 = Åk-poor part of lath at rim of inclusion; 5 = Åk-rich part of lath at rim of inclusion.

BDL: Below the detection limit of 0.017 wt% Na_2O or 0.025 wt% TiO_2; n.a.: not analyzed.

fine-grained, secondary alteration products that were probably derived from melilite. They are mainly grossular and nepheline with minor anorthite. The inclusion is rimmed by a thin (~10 μm) layer of FeO-bearing spinel and, outside that, a discontinuous layer of olivine (Fo_{60}). These layers and the abundance of fine-grained alteration products near the rim of the inclusion can be seen at the left edge of the view of the inclusion shown in Fig. 1d. The socket from which the inclusion came was examined in the SEM and additional rim layers were not found.

Mineral Chemistry

Melilite

We analyzed melilite laths at the rim of the inclusion, blocky grains in the core, and laths that extend from the core into the mantle. Representative analyses of melilite in each of these occurrences are presented in Table 1. The results of a representative electron probe traverse along the length of one of the rim laths shown in Fig. 1d are illustrated in Fig. 2. Assuming it nucleated at the rim of the inclusion, the grain is normally zoned over the first 400 μm of its length, with åkermanite contents increasing from about $Åk_{30}$ to about $Åk_{70}$ and reversely zoned over the last ~200 μm to crystallize to about $Åk_{50}$, probably due to cocrystallization with fassaite (MacPherson et al. 1984). With increasing distance from the rim of the inclusion, the contents of Na_2O (Fig. 2b) decrease for the first ~100 μm from the rim, reach a minimum, increase over the normally-zoned portion of the grain, and remain high throughout the reversely-zoned portion.

The small, blocky grains in the core are very strongly concentrically zoned. Most are normally zoned, but some are reversely zoned. The latter grains appear to have rounded, Åk-rich cores that are enclosed in normally-zoned overgrowths. The variety of zoning in the core grains is best seen in elemental X-ray maps and quantitative maps of åkermanite content. A representative area is shown in Fig. 3. Note the strong zoning of many of the grains. In the Al X-ray map (Fig. 3b), normally zoned grains have light cores and dark rims, while reversely zoned grains, several of which are indicated by arrows, have dark cores and light rims. Åkermanite contents can vary from $Åk_{30}$ to $Åk_{70}$ over a few tens of microns.

Also present in the core are fassaite-poor, melilite clusters rimmed by spinel grains. One of these clusters is shown in Fig. 4a. Figure 4b shows a quantitative map of åkermanite contents in melilite and TiO_2^{tot} (all Ti as TiO_2) contents in fassaite in the area shown in Fig. 4a. These clusters contain grains that are concentrically zoned from irregularly-shaped cores of about $Åk_{5–10}$ (red to orange) to rims that reach $Åk_{60–70}$ (green and blue) at their outermost parts. Similar textures and melilite zoning patterns were seen in other regions of the core that were mapped. It is unusual to find such gehlenitic melilite in the interior of a type B inclusion; it is usually only found at the extreme outer edge of an inclusion. It appears from Fig. 4b that the contacts between the cores and the overgrowths are sharp, and this is confirmed by the results of an electron probe traverse across two grains and their overgrowths within the cluster (Fig. 5). The location of the traverse is indicated by the arrowed line in Fig. 4a. Both gehlenitic grains analyzed, with compositions of $Åk_{~6–12}$ and Na_2O below the detection limit, are enclosed in melilite zoned

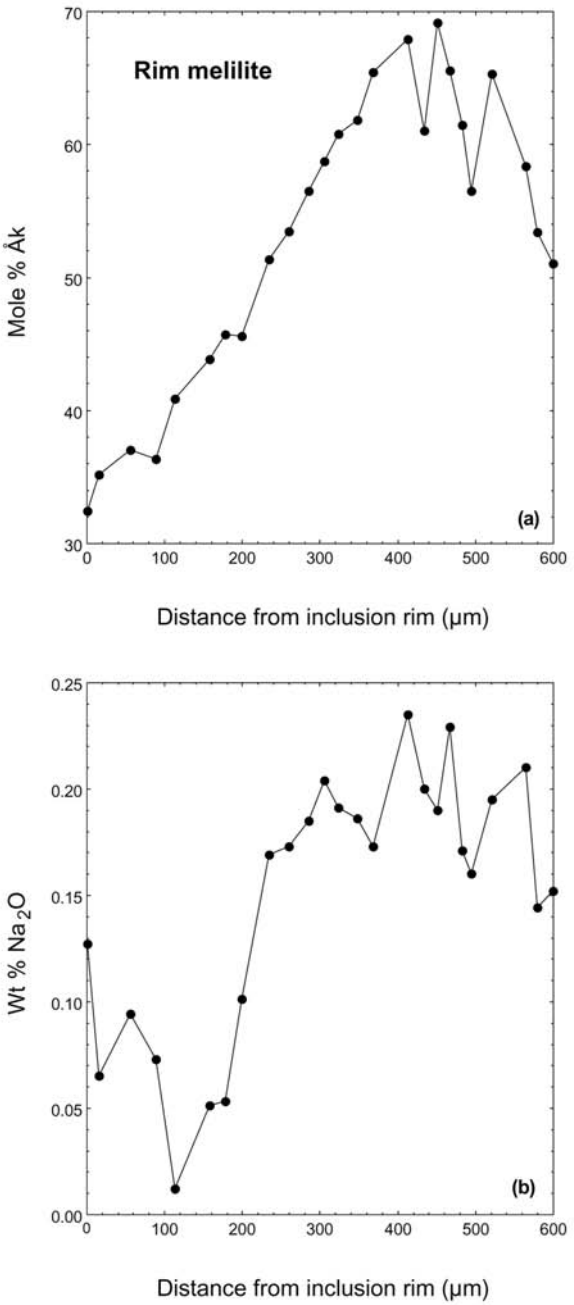

Fig. 2. Results of an electron probe traverse along the length of one of the mantle melilite grains shown in Fig. 1d: a) mole% åkermanite content versus distance from the rim of the inclusion; b) wt% Na_2O versus distance from the rim of the inclusion.

from $Åk_{\sim 15}$ to $Åk_{\sim 45}$, with Na_2O correlated with Åk and increasing from below detection to ~0.15 wt% over a distance of just 10–20 μm. If, as we explain below, the overgrowths belong to the same generation of melilite as the laths at the rim of the inclusion, then, like the laths, they should have begun crystallizing with a composition of $Åk_{\sim 30}$. This implies that the thin transitional zone (about 5 μm wide and labeled "TZ" in Fig. 5) between the gehlenitic grains and the

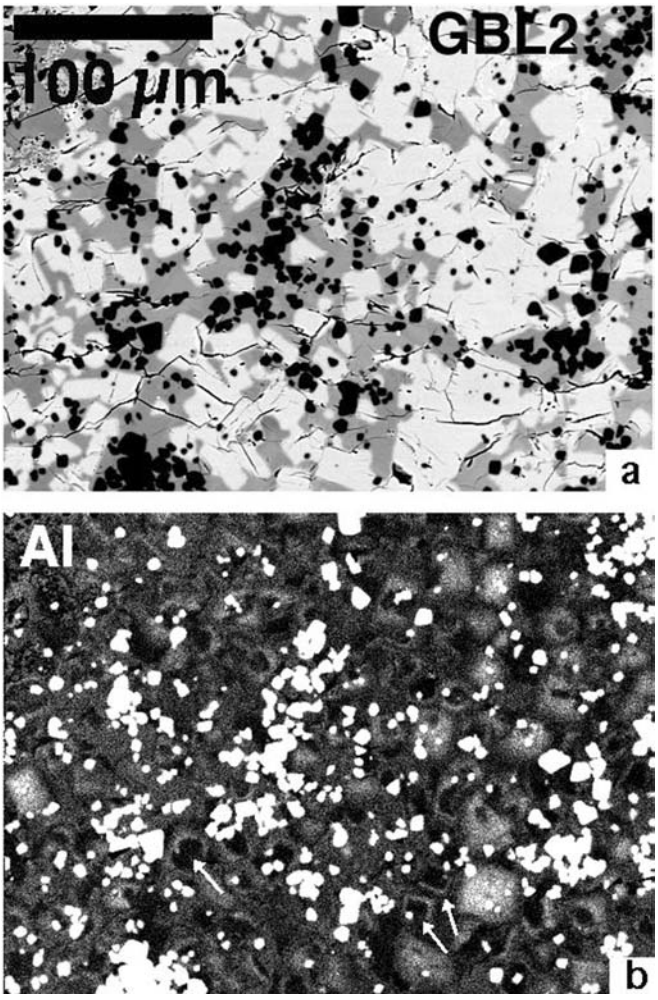

Fig. 3. a) Backscattered electron image of the core in section GBL2 and b) Al X-ray map of the same field of view. Arrows indicate grains with Al-poor cores (dark) and Al-rich rims (light).

overgrowths, with intermediate åkermanite contents and Na_2O contents that range from below detection to ~0.08 wt% Na_2O, reflects diffusion between the two generations of melilite. Alternatively, the intermediate composition of the TZ could reflect metastable, early crystallization of relatively gehlenitic melilite, just prior to nucleation of $Åk_{30}$ at the inclusion rim.

The third major occurrence of melilite in this inclusion is as the laths that are part of the core of the inclusion and extend into the mantle. We had difficulty performing electron probe traverses along the lengths of these grains because of the high abundance of secondary alteration products and spinel grains enclosed in these laths. The analyses and quantitative maps we could obtain show that these laths generally have fairly uniform compositions of $\sim Åk_{60}$ along their lengths, decreasing to $Åk_{45-55}$ in the outermost (i.e., furthest from the core) 100–150 μm. If these grains crystallized from the core of the inclusion outward, then they have reversely zoned rims.

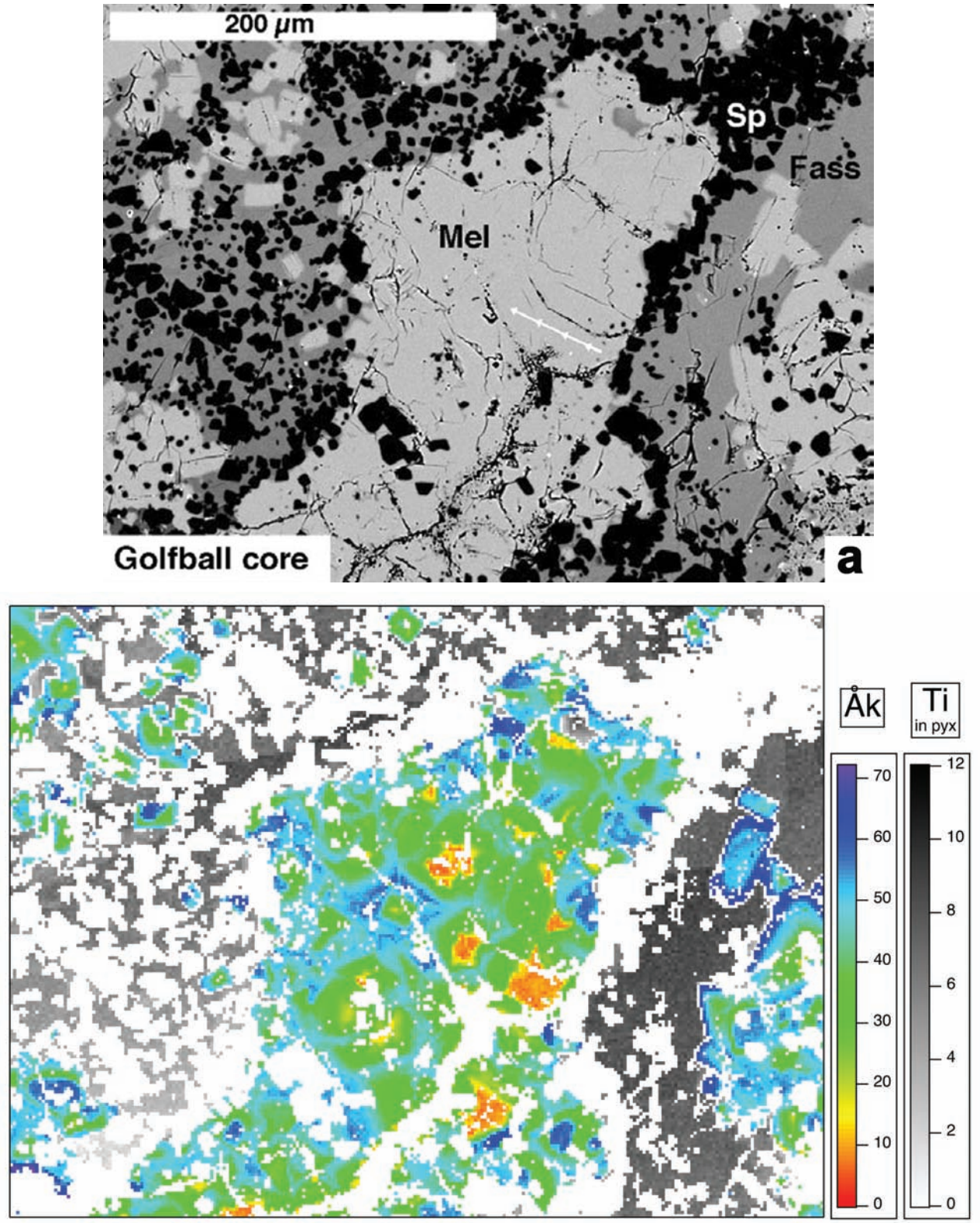

Fig. 4. a) Backscattered electron image of a fassaite-poor cluster of melilite grains in the core of GBL2. Arrowed line shows location of an electron probe traverse. b) Quantitative map of åkermanite contents in melilite and TiO_2 contents in fassaite for the area shown in (a). Note gehlenitic crystal cores (red) enclosed in strongly zoned, åkermanitic overgrowths, and that fassaite in contact with the cluster is relatively TiO_2-rich.

The Na_2O-åkermanite relationships in Golfball melilite are summarized in Fig. 6. Most of the gehlenitic melilite in the core has Na_2O contents below the detection limit of the electron probe. The other small grains in the core, $Åk_{20–65}$, are Na-bearing and yield a swath of analyses that has a positive slope on this plot. Analyses of the laths in the core overlap this trend at the high-åkermanite end, but the laths adjacent to the inclusion rim do not. The Åk-rich parts of the rim laths plot at the high end of the trend of the core melilite analyses. The Åk-poor parts of the rim laths ($Åk_{32–42}$) mostly plot below or above the interior melilite trend.

Fassaite

We analyzed coarse fassaite in the mantle and palisade body and pockets of fassaite in the core. Representative analyses are given in Table 2. The coarse fassaite is zoned with respect to Ti contents, either asymmetrically from one side to the other, or concentrically and decreasing from core to rim. Contents of Ti oxides range from ~9 wt% TiO_2 + Ti_2O_3 down to 1 wt% TiO_2^{tot} (values <<~4 wt% TiO_2^{tot} are too low for reliable calculation of separate TiO_2 and Ti_2O_3 contents). The maximum TiO_2^{tot} content in fassaite in a typical type B1 inclusion is ~12 wt%, so, like that in B2s, the fassaite in Golfball tends to be less strongly zoned than that in type B1s. Results of a representative electron probe traverse of a coarse fassaite grain from the mantle are illustrated in Fig. 7. As is typical of fassaite in type B inclusions, contents of Sc_2O_3 and V_2O_3 are correlated with each other and with Ti oxides. As shown in Fig. 7, however, although TiO_2 + Ti_2O_3 decreases smoothly from core to rim, the $Ti^{3+}/(Ti^{3+} + Ti^{4+})$ ratio does not. This is commonly seen in type B2 inclusions (Simon and Grossman 2003) and is different from what is observed in type B1 inclusions, in which $Ti^{3+}/(Ti^{3+} + Ti^{4+})$ tends to decrease monotonically from core to rim in fassaite crystals, along with TiO_2 + Ti_2O_3, V_2O_3, and Sc_2O_3 (Simon et al. 1991).

The poikilitic fassaite in the core has ranges of contents of these oxides that are very similar to those of the mantle fassaite. Within the small area shown in Fig. 4b, TiO_2^{tot} contents in fassaite range from ~9 to <2 wt%. In Golfball fassaite, Sc_2O_3 contents (Fig. 8a) are below the detection limit of the electron microprobe (0.03 wt%) in all fassaite with TiO_2 + Ti_2O_3 < ~4.5 wt%, and reach 0.16–0.19 wt% in fassaite with >6 wt% TiO_2 + Ti_2O_3. Analyses of mantle, poikilitic, and palisade body fassaite all fall on this general trend. Figure 8b shows that there are detectable amounts of V_2O_3 in almost all of our fassaite data. Analyses of mantle and poikilitic fassaite fall on a single trend, which ranges from 0.12–0.17 wt% V_2O_3 at ~2 wt% TiO_2 + Ti_2O_3 up to ~0.40 wt% V_2O_3 at ~8 wt% TiO_2 + Ti_2O_3. A strongly-zoned grain in the palisade body has a wider range of V_2O_3 contents than this, from 0.03–0.52 wt%. Data for this grain are plotted separately in Fig. 8. Except for this grain, the mantle and poikilitic fassaite tend to have higher V_2O_3 contents than that in the palisade body. This could be due to local V-enrichment of the melt by oxidation of V metal originally contained in Fremdlinge (Blum et al. 1989), which are common in the mantle fassaite. The palisade body also contains abundant

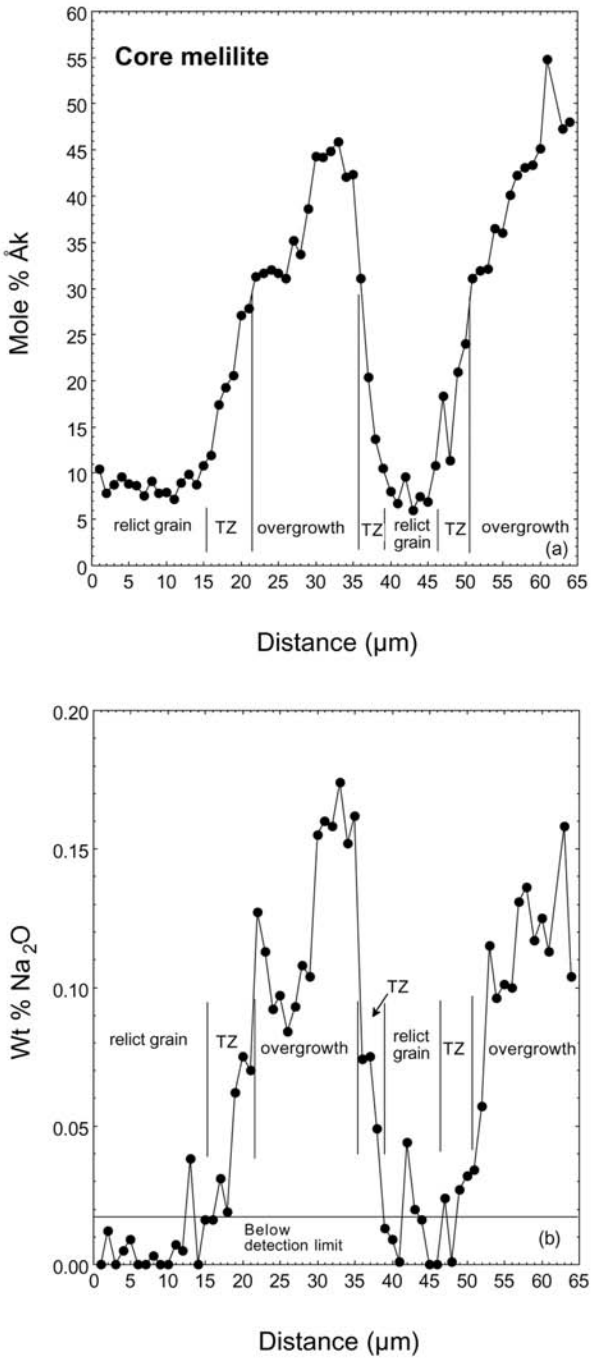

Fig. 5. Results of an electron probe traverse across two gehlenitic grains and their overgrowths in the core of Golfball: a) mole% åkermanite content versus distance; b) wt% Na_2O versus distance. Vertical lines indicate approximate extents of relict grains, overgrowths and the transitional zones (TZ) between them.

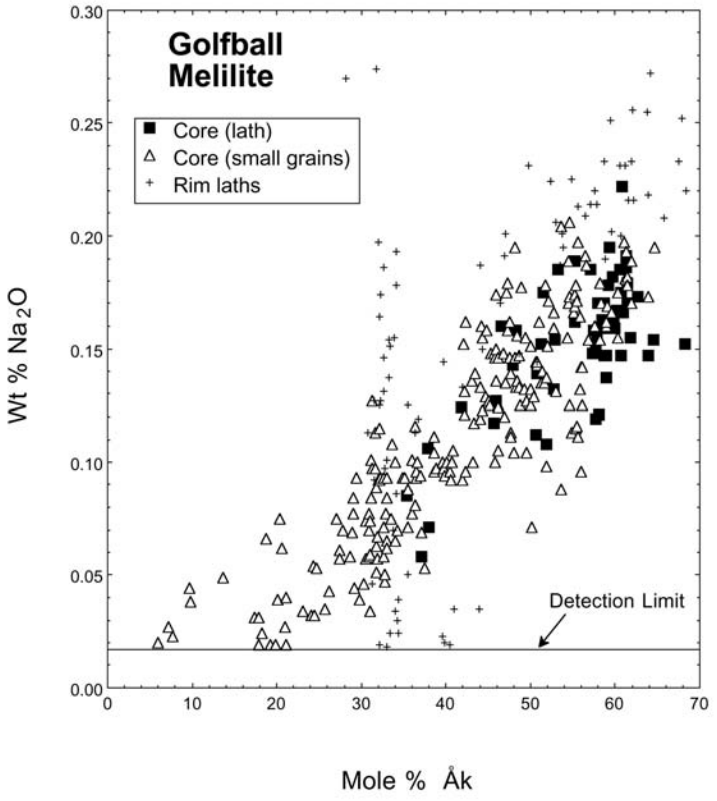

Fig. 6. Plot of wt% Na_2O versus mole% åkermanite for melilite in Golfball. There is a strong correlation except for the laths immediately adjacent to the rim of the inclusion, which probably reflects late diffusion of Na into the inclusion. Most of the melilite with $Åk_{<15}$ and portions of the rim laths have Na_2O contents that are below the detection limit of the electron probe (these data are not plotted).

Fremdlinge, but most of them are enclosed in melilite, not in fassaite.

Spinel

Spinel is quite abundant in this inclusion. It is nearly pure $MgAl_2O_4$ with minor amounts of TiO_2 and V_2O_3. The abundances of these oxides in spinel are plotted in Fig. 9, with different symbols based upon the locations of the spinel. Representative analyses of spinel from each of these occurrences are given in Table 3. The relationships between spinel composition and location in the inclusion are like those documented by Connolly et al. (2003) in TS34, a type B1 inclusion from Allende. Spinel enclosed in fassaite is enriched in TiO_2 relative to that enclosed in melilite. Spinel enclosed in the poikilitic fassaite pockets in the core tends to have lower TiO_2 contents than that enclosed in the coarse fassaite in the mantle. We also found, as did Connolly et al. (2003), that spinel enclosed in melilite near the edge of the inclusion tends to have the highest V_2O_3 contents. Spinel enclosed in melilite in the core of the inclusion has low V_2O_3 and TiO_2 contents. The coarse, framboidal spinel has intermediate V_2O_3 contents and a wide range of TiO_2 contents.

DISCUSSION

Formation of Golfball

Any model for the formation of this inclusion must not only account for the existence of a melilite-rich core in a type B inclusion, but also for the presence in the core of melilite that is more gehlenitic than that at the rim of the inclusion. Important constraints are provided by the inclusion bulk composition, the melilite and fassaite occurrences, and melilite Åk and Na_2O contents.

Beckett et al. (1999) calculated contours of initial melilite compositions for spinel-saturated liquid compositions that project from Spinel into the melilite + spinel field of the Gehlenite-Anorthite-Forsterite plane in the CMAS system. Because Golfball is a zoned object, its bulk composition (Simon and Grossman 2004) was calculated from the weight proportions of its mantle and core. The compositions of these components and the bulk sample are plotted with the contours of Beckett et al. (1999) in Fig. 10. Compositions of other type B inclusions (Simon and Grossman 2004) are shown for reference. Golfball is slightly MgO-rich relative to other type B inclusions, but, despite its

Table 2. Representative electron probe analyses of fassaite in Golfball.

	1	2	3	4	5	6
MgO	9.59	11.99	11.82	9.39	9.66	12.01
Al_2O_3	18.00	15.29	16.22	18.97	19.51	15.55
SiO_2	39.06	42.34	43.87	38.54	39.44	44.77
CaO	25.41	25.21	25.77	25.32	25.62	25.57
Sc_2O_3	0.13	0.07	BDL	0.08	BDL	BDL
TiO_2	7.66	5.14	2.21	7.28	5.33	1.72
V_2O_3	0.33	0.31	0.20	0.38	0.21	0.15
Cr_2O_3	0.05	0.06	0.09	0.07	0.10	0.07
FeO	BDL	0.03	0.03	0.03	BDL	0.09
Sum	100.24	100.42	100.20	100.07	99.90	99.91
Ti_2O_3	4.35	1.00	n.d.	3.68	2.46	n.d.
TiO_2	2.88	3.98	n.d.	3.22	2.64	n.d.
Sum	99.81	100.27	100.20	99.69	99.67	99.91
	Cations per 6 oxygen anions					
Si	1.451	1.541	1.595	1.430	1.459	1.627
Al	0.549	0.459	0.405	0.570	0.541	0.373
oct Al	0.239	0.196	0.290	0.261	0.310	0.293
Mg	0.531	0.650	0.641	0.520	0.532	0.651
Fe	0	0.001	0.001	0.001	0	0.003
Sc	0.004	0.002	0	0.003	0	0
V	0.009	0.008	0.005	0.011	0.006	0.004
Cr	0.002	0.002	0.003	0.002	0.003	0.002
Ti^{3+}	0.134	0.031	n.d.	0.114	0.075	n.d.
Ti^{4+}	0.080	0.110	0.061	0.090	0.073	0.047
Ti^{3+}/Ti^{tot}	0.627	0.218	n.d.	0.559	0.508	n.d.

1–3 = Coarse mantle fassaite; 4–6 = poikilitic core fassaite. Analyses are normalized to four cations, including two tetrahedral and one Ca cation per six oxygen anions, according to the methods of Beckett (1986).
BDL = Below detection limit of 0.03 wt% FeO or Sc_2O_3; n.d.: not determined.

Table 3. Representative analyses of spinel in different occurrences in Golfball.

	1	2	3	4
MgO	28.64	28.57	28.41	28.61
Al_2O_3	70.32	69.89	69.75	69.94
SiO_2	0.03	0.06	0.08	BDL
CaO	0.18	0.32	0.11	0.07
Cr_2O_3	0.22	0.20	0.29	0.12
TiO_2	0.16	0.30	0.43	0.23
V_2O_3	0.30	0.56	0.37	0.40
FeO	0.10	0.08	0.27	0.03
Total	99.95	99.98	99.71	99.41
	Cations per four oxygen anions			
Mg	1.015	1.013	1.010	1.019
Al	1.971	1.961	1.962	1.970
Si	0.001	0.001	0.002	0
Ca	0.005	0.008	0.003	0.002
Cr	0.004	0.004	0.005	0.002
Ti	0.003	0.005	0.008	0.004
V	0.006	0.011	0.007	0.008
Fe	0.002	0.002	0.005	0.001
Total cations	3.007	3.005	3.002	3.006

1 = In gehlenitic melilite in the core; 2 = in a melilite lath at the rim of the inclusion; 3 = in mantle fassaite; 4 = coarse spinel in a framboid.
BDL: Below detection limit of 0.013 wt% SiO_2.

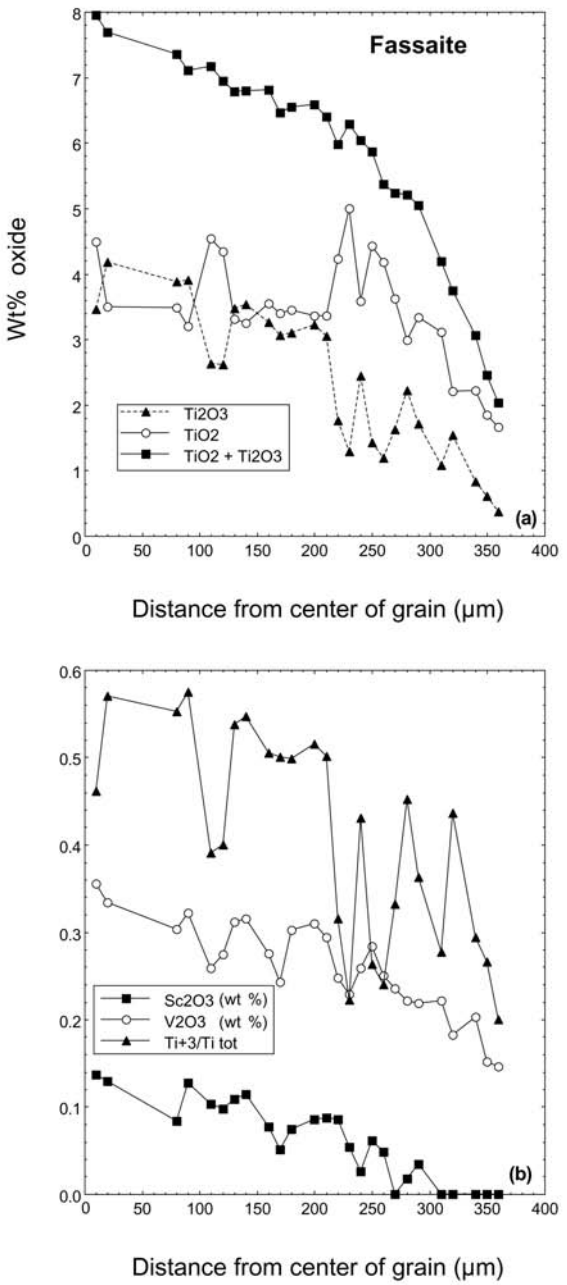

Fig. 7. Results of a core-to-rim electron probe traverse across a coarse fassaite grain in the mantle of Golfball: a) Ti oxides; b) Sc_2O_3 (wt%), V_2O_3 (wt%), and $Ti^{3+}/(Ti^{3+} + Ti^{4+})$.

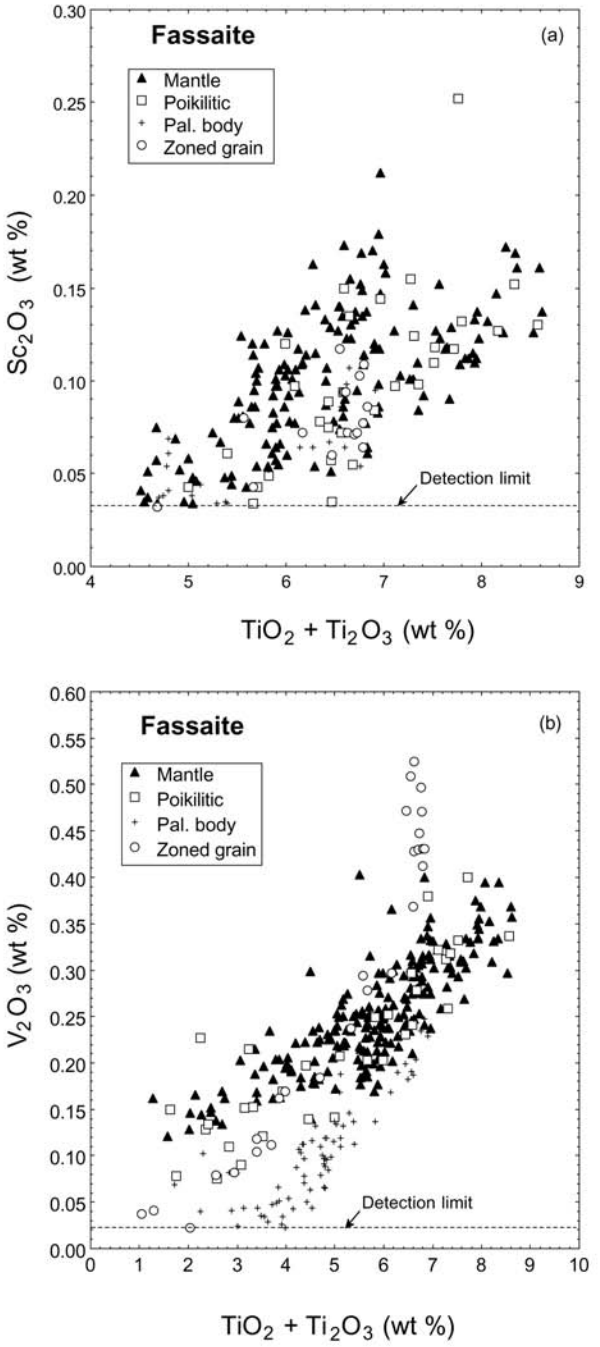

Fig. 8. Minor element contents of fassaite in Golfball, by petrographic occurrence: a) wt% Sc_2O_3 versus $Ti_2O_3 + TiO_2$; b) wt% V_2O_3 versus $Ti_2O_3 + TiO_2$. Mantle: coarse grains in the mantle; Poikilitic: poikilitic fassaite in the core; Pal. body: palisade body; Zoned grain: zoned grain in palisade body. Only analyses that are above the detection limits of the electron microprobe for the oxide plotted are shown.

unique texture, it does not have an anomalous bulk composition. This indicates that Golfball formed from an assemblage of precursor grains that was typical for type B inclusions. The gehlenitic melilite ($Åk_{\leq 12}$) in the core of Golfball clearly could not have formed from a liquid having either the composition of bulk Golfball or even that of its core. These grains must be relict, and they probably represent the earliest generation of material found in Golfball.

A sequence of major events that accounts for the chemical and petrographic features of Golfball is illustrated in Fig. 11. In the first heating event, most of the precursor assemblage melted. Some of the spinel and the gehlenitic melilite ($Åk_{\leq 12}$) did not melt, and these grains became loosely

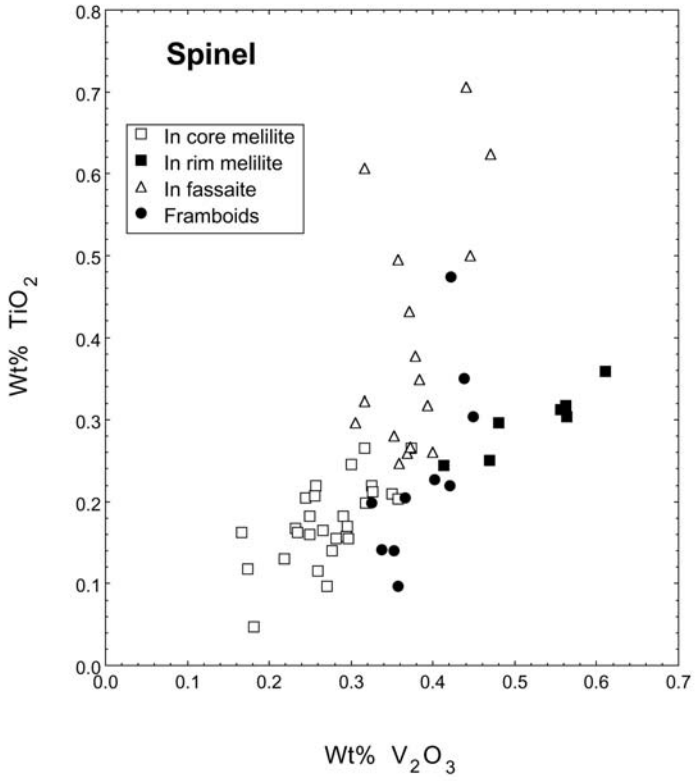

Fig. 9. Contents of V_2O_3 and TiO_2 in spinel in Golfball by petrographic occurrence.

concentrated in the core. This is illustrated in the first panel of Fig. 11.

Upon cooling of this melt, step 2 in Fig. 11, a new generation of Na-poor melilite crystallized. This melilite is represented by the diagonal line pattern in Fig. 11. It nucleated as laths at the rim of the inclusion with compositions of $Åk_{30}$ and <0.02 wt% Na_2O. In this melilite, Na_2O contents decrease inward from the rim of the inclusion and reach minima (Fig. 2) below the detection limit of the electron probe. We interpret the low Na_2O contents as primary and the high Na_2O contents near the rim as secondary, reflecting late diffusion into the inclusion. In addition, as depicted in Fig. 11, it is likely that in this step melilite also nucleated on relict grains in the core, although we note that the innermost approximately 5 μm of the overgrowths ("TZ" in Fig. 5) have lower åkermanite (15–30 mole%) contents than the inferred initial composition of the laths at the rim. If $Åk_{30}$ grew simultaneously at the inclusion rim and upon relict grains in the core, then the intermediate compositions of the transitional zone could reflect diffusional exchange between the two generations of melilite (i.e., the relict grains and the overgrowths). The presence in the TZ, however, of melilite with elevated Åk contents and Na_2O contents below detection would require that diffusion of Mg from the overgrowth was faster than that of Na, and this does not seem likely. This suggests an alternate explanation, that a) the overgrowths nucleated metastably and early on the relict grains in the core, before the laths at the rim began to grow, and b) Na_2O partially diffused into this melilite from the later-formed, Na_2O-bearing melilite.

In step 3, after the Na_2O-poor melilite formed, and probably after solidification of the remainder of the melt, the inclusion underwent open system, secondary alteration and Na was introduced. Melting then occurred again, but the inclusion was not as strongly heated as it was the first time, as melilite with Åk contents of up to ~40 mol% did not melt. This is indicated by zoning profiles of laths at the rim; as illustrated in Fig. 2, the portions of these grains with åkermanite contents <40 mol% have low Na_2O contents. In addition, traverses of this and several other rim melilites show that with respect to åkermanite contents, these grains tend to be unzoned to weakly zoned between $Åk_{30}$ and $Åk_{35}$ but strongly zoned from $Åk_{40–65}$.

In step 4, during cooling following this heating event, Na-bearing melilite, represented by the stippled areas in Fig. 11, crystallized from the melt. This melilite occurs as overgrowths on the initially Na-free melilite in the core and at the rim. In addition, many small, strongly-zoned melilite grains also formed in the core, probably due to the preservation of abundant nuclei as a result of the relatively low peak temperature. Laths nucleated on the core of the inclusion and grew outward into the molten mantle. Although spinel was present, it tended to be excluded from the melilite, as is commonly observed in early melilite in type B

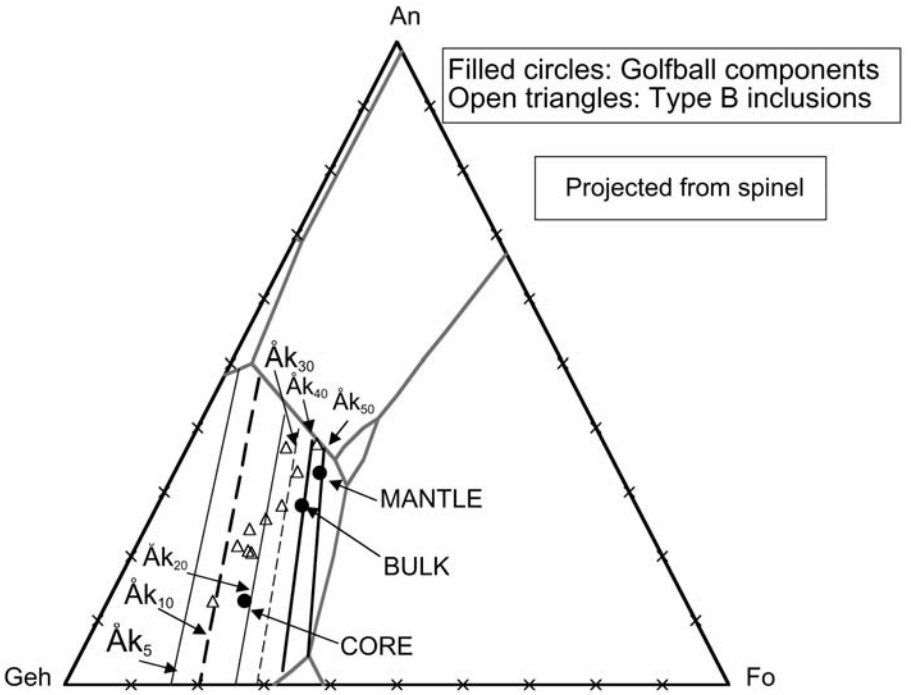

Fig. 10. Projection of the core, mantle, and bulk compositions of Golfball from spinel onto the Gehlenite-Anorthite-Forsterite plane of the CMAS system, using the method of Stolper (1982). From the contours of åkermanite contents of earliest melilite (Beckett et al. 1999), the gehlenitic melilite found in the core would not be expected to crystallize from a melt of the bulk inclusion or even just the core. Compositions of other type B inclusions (Simon and Grossman 2004) are shown for reference.

inclusions, especially in the mantles of B1s. Next, fassaite (vertical lines in Fig. 11) crystallized from the residual melt, mainly in the mantle of the inclusion, but also in pockets in the core, poikilitically enclosing relict melilite grains and their overgrowths, individual blocky grains, and spinel. When fassaite crystallization caused the MgO/Al_2O_3 ratio of the residual melt to decrease, the cocrystallizing melilite became reversely zoned (MacPherson et al. 1984), as is observed in the outer margins of laths and some blocky grains that are enclosed in fassaite. Finally, the inclusion was altered again, forming the secondary alteration products now present and giving rise to the gradient of decreasing Na_2O contents, with increasing distance from the rim of the inclusion, within melilite at the rim. This likely represents late, inward diffusion of Na_2O into the melilite. Diffusion also smoothed contacts between Na-free and Na-bearing melilite.

Estimates of Peak Temperatures of Melting Events

The texture and zoning patterns of the phases in Golfball are consistent with at least two melting events while the inclusion was in the nebula. As the temperature reached by the melts in such events increases, the maximum åkermanite content of the unmelted melilite decreases. Therefore, the earliest melting event, which only spinel and gehlenitic melilite survived, must have reached a higher temperature than the later one.

Dynamic crystallization experiments (e.g., Stolper and Paque 1986) show that the textures of coarse-grained CAIs require that they crystallized from a partially molten state. It is therefore fairly widely accepted that when CAIs were melted, their temperatures did not exceed the equilibrium appearance temperature of melilite in an average type B composition, ~1400 °C (Stolper 1982), by more than several tens of degrees or for an extended period of time. Otherwise, melilite crystal nuclei would have been destroyed, which would have resulted in crystallization of skeletal or dendritic melilite, which is not observed in CAIs, including Golfball. The presence of relict melilite in Golfball also precludes extended heating well above the appearance temperature of melilite, but since almost all melilite in Golfball was indeed melted, its temperature probably did approach 1400 °C during the early melting event.

For the last melting event experienced by Golfball, we can estimate the crystallization temperature of the first melilite (~$Åk_{40}$) from the temperature-Åk trend derived from numerous experiments on the CAIB composition (Stolper 1982), compiled by Beckett et al. (1999). When we do so, a temperature of ~1260 °C is obtained. In this melting event, Na_2O was present and partitioned between the melt and melilite, giving rise to the positive Na_2O-Åk correlation that is observed in the rim laths.

Probably the first evidence suggesting that an inclusion was melted after being altered was reported by MacPherson

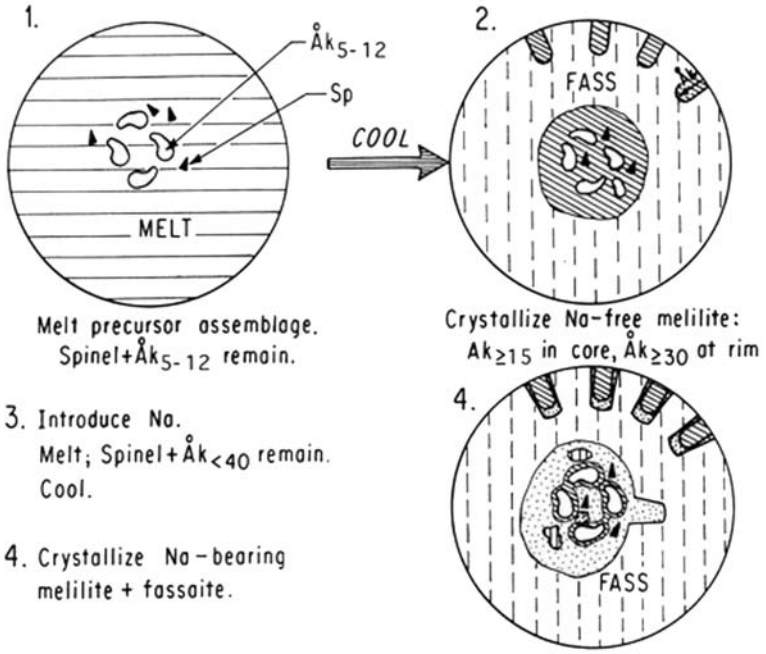

Fig. 11. Summary of the major events in the development of Golfball. Crystals, such as those at the rim of the inclusion, are not drawn to scale. No pattern = relict gehlenitic melilite in the core; diagonal lines = Na-free melilite that crystallized after the first melting event; stippled pattern = Na-bearing melilite formed after the second melting event. Note overgrowths on mantle and core melilite, including representation of a lath protruding from the core into the mantle.

and Davis (1993) in their thorough study of 1623-8, a type B inclusion from Vigarano. They found that, although the inclusion is now lightly altered, as are most CAIs from the reduced subgroup of CV3s, the melilite in 1623-8 has high Na_2O contents that are strongly correlated with Åk contents. This led MacPherson and Davis to suggest that Na_2O was present in the parental melt and that it was formed from precursor solids that were Na-bearing. This concept was supported by a study of Allende type B1 inclusion TS34 by Beckett et al. (2000). This inclusion, like Golfball and 1623-8, has early, relatively gehlenitic melilite with such low Na contents that it indicates formation from an essentially Na-free source, while later melilite is Na-bearing, with zoning that can be accounted for by fractional crystallization models (Beckett et al. 2000) based on experimentally determined (Beckett and Stolper 2000) melilite/liquid distribution coefficients.

These three inclusions, with well-documented igneous zoning of Na in melilite, also have Mg that is isotopically heavy, as determined by thermal ionization mass spectrometry for 1623-8 (Loss et al. 1994) and by multi-collector ICP-MS for TS34 and Golfball (Simon et al. 2004). The bulk Mg isotopic compositions of 1623-8, TS34, and Golfball show enrichment in ^{25}Mg by 12.2 ± 0.5, 5.63 ± 0.28, and 1.61 ± 0.06 ‰/amu, respectively, relative to the DSM3 standard (Galy et al. 2003). Assuming that these isotopic compositions are due to evaporation-induced mass-fractionation of Mg rather than nebular heterogeneity, they correspond to a range of evaporative losses from several percent to several tens of percent, at least, of the Mg originally present. Because Na is much more volatile than Mg in cosmic gases, it would also evaporate during any event in which Mg is lost. Golfball and 1623-8 have very different Mg isotopic compositions, but the average Na_2O contents of their melilite are virtually identical: 0.17 wt% in 1623-8 (MacPherson and Davis 1993) and 0.14 wt% in Golfball, and are somewhat higher than TS34 (~0.09 wt%). The ranges of Na_2O contents in melilite in all three inclusions are similar, from ~0.3 wt% to below detection. As there is no correlation between Na_2O contents of melilite and the degree of Mg loss, the events that caused isotopic fractionation of Mg must be distinct from the ones during which Na-bearing melilite crystallized.

A pattern of thermal histories involving multiple melting events is emerging from a variety of detailed observations of coarse-grained CAIs, with one event at ~1400 °C and a later one at 1250–1300 °C. Several studies have reached similar conclusions for a variety of reasons. Davis et al. (1991) found both normal ($Åk_{16–60}$) and extremely åkermanitic ($Åk_{99}$) melilite in a forsterite-rich FUN CAI, Vigarano 1623-5, and presented petrologic and isotopic evidence for a late flash-heating event that melted the outer portions of the CAI. Lin and Kimura (2000) also found both typical ($Åk_{<70}$) and åkermanitic ($Åk_{70–90}$) melilite in a type B inclusion. They concluded that a mild reheating event that generated a melt with a low Al/Mg ratio best accounted for the occurrence of

extremely magnesian melilite. Another example of a remelted inclusion was reported by Ito et al. (2004), who conducted a thorough ion probe study of the oxygen isotopic compositions in a compact type A inclusion from Allende. They found that the wide range of compositions among the different phases and within single crystals of melilite was best explained by formation of the inclusion in an ^{16}O-rich environment, followed by melting and crystallization in a relatively ^{16}O-poor one. Finally, four thorough studies of USNM 5241, a type B1 with fassaite-rich "spinel-free islands," suggest a complex thermal history for that inclusion as well. Two studies (El Goresy et al. 1985; MacPherson et al. 1989) interpret the islands as xenoliths that became enclosed in a later-formed melt. Davis et al. (1998) found that large fassaite crystals have three zones with contrasting interelement ratios, which they concluded corresponded to remelting episodes that yielded melts with slightly different compositions from each other. In an Al-Mg isotopic study, Hsu et al. (2000) reported different ages for the petrographic components of 5241, with the islands being the oldest, followed by the core of the inclusion and the melilite mantle. From their data, they conclude that the formation of these components occurred over a period of 4×10^5 yr.

The studies of 5241 and those by MacPherson and Davis (1993), Beckett et al. (2000), Davis et al. (1991), Lin and Kimura (2000), and Ito et al. (2004) present different types of strong evidence for remelting in a total of six CAIs. Although Golfball has a unique structure among known CAIs, its thermal history may not have been anomalous.

Significance of Golfball

An inclusion unlike any that has been seen before has been found in one of the most thoroughly studied meteorites. If new types of inclusions can be found in Allende, then it is likely that new types can be found in most other carbonaceous chondrites as well. New types that add to the range of textures or observed mineral assemblages or compositions could help place new constraints on the conditions of condensation of CAI precursors, or, like Golfball, they might record evidence of thermal histories either not experienced or recorded by other refractory inclusions, thereby improving our understanding of the variability of conditions in the early solar nebula.

CONCLUSIONS

We have described herein a unique inclusion from Allende. It is a type B inclusion with a melilite-rich core and a fassaite-rich mantle, with melilite laths at the edge of the core and oriented at high angles to it in addition to radially oriented melilite laths at the inclusion rim. Small grains of relict, gehlenitic melilite are also present in the core and are enclosed in strongly zoned overgrowths. The texture of the inclusion and zoning of the melilite appear to record two melting events. In the first event, the inclusion completely melted except for gehlenitic ($Åk_{\leq 12}$) melilite and some spinel. As the inclusion cooled, Na-free melilite crystallized in the core and at the rim. The inclusion underwent secondary alteration and was melted again. This time the peak temperature was lower than that of the earlier event and melilite with Åk contents up to 40 mol% did not melt. Upon cooling, Na-bearing melilite crystallized, followed by fassaite. Cocrystallization of melilite and fassaite led to reverse zoning of the outer margins of melilite laths. The inclusion was eventually altered again, giving rise to the secondary alteration products present in the inclusion. The coexistence of Na-free and Na-bearing melilite, correlation of Na_2O and åkermanite contents of melilite in the presence of Mg that is mass-fractionated in favor of the heavy isotopes, and an absence of a correlation between Na_2O contents in melilite and degree of Mg isotopic fractionation in this and two other type B inclusions all provide clear evidence for two melting events in the histories of these inclusions. The earlier one was a high-temperature event during which evaporative loss of Mg occurred, and the later one was at temperatures low enough that Na remained in the melt.

Acknowledgments–We thank E. Poole for skillfully drafting Fig. 11 and I. M. Steele for maintaining the electron probe. S. Russell and A. N. Krot provided helpful reviews. This work was funded by the National Aeronautics and Space Administration through grants NAG-11588 (LG) and NAG5-12997 (AMD), and funding is gratefully acknowledged.

Editorial Handling—Dr. Allan Treiman

REFERENCES

Beckett J. R. 1986. The origin of calcium-, aluminum-rich inclusions from carbonaceous chondrites: An experimental study. Ph.D. thesis, The University of Chicago, Chicago, Illinois, USA.

Beckett J. R. and Stolper E. 2000. The partitioning of Na between melilite and liquid: Part I. The role of crystal chemistry and liquid composition. *Geochimica et Cosmochimica Acta* 64:2509–2517.

Beckett J. R., Paque J. M., and Stolper E. 1999. The use of melilite compositions to constrain the thermal history and liquid line of descent of type B CAIs (abstract #1920). 30th Lunar and Planetary Science Conference. CD-ROM.

Beckett J. R., Simon S. B., and Stolper E. 2000. The partitioning of Na between melilite and liquid: Part II. Applications to type B inclusions from carbonaceous chondrites. *Geochimica et Cosmochimica Acta* 64:2519–2534.

Blum J. D., Wasserburg G. J., Hutcheon I. D., Beckett J. R., and Stolper E. M. 1989. Origin of opaque assemblages in C3V meteorites: Implications for nebular and planetary processes. *Geochimica et Cosmochimica Acta* 53:543–556.

Connolly H. C. Jr., Burnett D. S. and McKeegan K. D. 2003. The petrogenesis of type B1 Ca-Al-rich inclusions: The spinel perspective. *Meteoritics & Planetary Science* 38:197–224.

Davis A. M., MacPherson G. J., Clayton R. N., Mayeda T. K., Sylvester P. J., Grossman L., Hinton R. W., and Laughlin J. R. 1991. Melt solidification and late-stage evaporation in the

evolution of a FUN inclusion from the Vigarano C3V chondrite. *Geochimica et Cosmochimica Acta* 55:621–637.

Davis A. M., Simon S. B., and Grossman L. 1998. Re-examination of the Allende type B1 CAI NMNH 5241 (abstract #1948). 29th Lunar and Planetary Science Conference. CD-ROM.

Dowty E. and Clark J. R. 1973. Crystal structure refinement and optical properties of a Ti^{3+} fassaite from the Allende meteorite. *American Mineralogist* 58:230–242.

El Goresy A., Nagel K., and Ramdohr P. 1979. Spinel framboids and fremdlinge in Allende inclusions: Possible markers in the early history of the solar system. Proceedings, 10th Lunar and Planetary Science Conference. pp. 833–850.

El Goresy A., Armstrong J. T., and Wasserburg G. J. 1985. Anatomy of an Allende coarse-grained inclusion. *Geochimica et Cosmochimica Acta* 49:2433–2444.

Galy A., Yoffe O., Janney P. E., Williams R. W., Cloquet C., Alard A., Halicz L., Wadhwa M., Hutcheon I. D., Ramon E., and Carignan J. 2003. Magnesium isotope heterogeneity of the isotopic standard SRM980 and new reference materials for magnesium-isotope-ratio measurements. *Journal of Analytical Atomic Spectrometry* 18:1352–1356.

Grossman L., Ebel D. S., Simon S. B., Davis A. M., Richter F. M., and Parsad N. M. 2000. Major element chemical and isotopic compositions of refractory inclusions in C3 chondrites: The separate roles of condensation and evaporation. *Geochimica et Cosmochimica Acta* 64:2879–2894.

Grossman L., Ebel D. S., and Simon S. B. 2002. Formation of refractory inclusions by evaporation of condensate precursors. *Geochimica et Cosmochimica Acta* 66:145–161.

Hsu W., Wasserburg G. J., and Huss G. R. 2000. High time resolution by use of the ^{26}Al chronometer in the multistage formation of a CAI. *Earth and Planetary Science Letters* 182:15–29.

Ito M., Nagasawa H., and Yurimoto H. 2004. Oxygen isotopic SIMS analysis in Allende CAI: Details of the very early thermal history of the solar system. *Geochimica et Cosmochimica Acta* 68:2905–2923.

Lin Y. and Kimura M. 2000. Two unusual type B refractory inclusions in the Ningqiang carbonaceous chondrite: Evidence for relicts, xenoliths, and multi-heating. *Geochimica et Cosmochimica Acta* 64:4031–4047.

Loss R. D., Lugmair G. W., Davis A. M., and MacPherson G. J. 1994. Isotopically distinct reservoirs in the solar nebula: Isotope anomalies in Vigarano meteorite inclusions. *Astrophysical Journal* 436:L193–L196.

MacPherson G. J. and Davis A. M. 1993. A petrologic and ion microprobe study of a Vigarano type B refractory inclusion: Evolution by multiple stages of alteration and melting. *Geochimica et Cosmochimica Acta* 57:231–243.

MacPherson G. J., Paque J. M., Stolper E., and Grossman L. 1984. The origin and significance of reverse zoning in melilite from Allende type B inclusions. *Journal of Geology* 92:289–305.

MacPherson G. J., Crozaz G., and Lundberg L. L. 1989. The evolution of a complex type B Allende inclusion: An ion microprobe trace element study. *Geochimica et Cosmochimica Acta* 53:2413–2427.

Pouchou J. L. and Pichoir F. 1984. A new model for quantitative X-ray microanalysis. Part I: Application to the analysis of homogeneous samples. *La Recherche Aerospatiale* 3:13–38.

Richter F. M., Davis A. M., Ebel D. S., and Hashimoto A. 2002. Elemental and isotopic fractionation of type B CAIs: Experiments, theoretical considerations, and constraints on their thermal evolution. *Geochimica et Cosmochimica Acta* 66:521–540.

Simon S. B. and Grossman L. 2003. Composition and zoning of fassaite in type B2 refractory inclusions (abstract). *Geochimica et Cosmochimica Acta* 67:A437.

Simon S. B. and Grossman L. 2004. A preferred method for the determination of bulk compositions of coarse-grained refractory inclusions and some implications of the results. *Geochimica et Cosmochimica Acta* 68:4237–4248.

Simon S. B., Grossman L., and Davis A. M. 1991. Fassaite composition trends during crystallization of Allende type B refractory inclusion melts. *Geochimica et Cosmochimica Acta* 55:2635–2655.

Simon S. B., Davis A. M., and Grossman L. 2002. Golfball, a large Allende type B inclusion with evidence for multiple stages of remelting (abstract). *Meteoritics & Planetary Science* 37:A130.

Simon S. B., Grossman L., Hutcheon I. D., Williams R. W., Galy A., Fedkin A. V., Clayton R. N., and Mayeda T. K. 2004. Determination of primordial refractory inclusion compositions (abstract #1684). 35th Lunar and Planetary Science Conference. CD-ROM.

Stolper E. 1982. Crystallization sequences of Ca-Al-rich inclusions from Allende: An experimental study. *Geochimica et Cosmochimica Acta* 46:2159–2180.

Stolper E. and Paque J. M. 1986. Crystallization sequences of Ca-Al-rich inclusions from Allende: The effects of cooling rate and maximum temperature. *Geochimica et Cosmochimica Acta* 50:1785–1806.

Wark D. A. and Lovering J. F. 1982. Evolution of Ca-Al-rich bodies in the earliest solar system: Growth by incorporation. *Geochimica et Cosmochimica Acta* 46:2595–2607.